



Original Article

Novel untethered micro-robotic platform developed for minimally invasive ultra-selective microsurgical procedures and targeted drug delivery: Preliminary characterization of tissue response to intraparenchymal navigation in ovine brain

William Loudon¹, Michael Kardosh^{2,3}, Florent Cros², Be'eri Katznelson^{3,4}, Aviv Shtein^{3,4}, Katerina Fedotenko³, Didi Castel⁴, Olin J. Palmer², Alexander Kiselyov²

¹Department of Neurosurgery, Children's Hospital Orange County, Orange, California, United States, ²Department of Research and Development, Bionaut Labs Inc., Culver City, ³Department of Engineering, Tel Aviv University, Tel Aviv, Dan, ⁴Department of Research and Development, Leviev Heart Center at Sheba Medical Center, Ramat Gan, Israel.

E-mail: *William Loudon - wloudon@choc.org; Michael Kardosh - michael.kardosh@bionautlabs.com; Florent Cros - florent.cros@bionautlabs.com; Be'eri Katznelson - katzbary@gmail.com; Aviv Shtein - aviv.shtein@bionautlabs.com; Katerina Fedotenko - fedotkatya@gmail.com; Didi Castel - casteldav@gmail.com; Olin J. Palmer - olin@olinpalmer.com; Alexander Kiselyov - alex.kiselyov@bionautlabs.com



***Corresponding author:**

William Loudon,
Department of Neurosurgery,
Children's Hospital Orange
County, Orange, California,
United States.

wloudon@choc.org

Received: 07 October 2024

Accepted: 23 January 2025

Published: 02 May 2025

DOI

10.25259/SNI_841_2024

Quick Response Code:



ABSTRACT

Background: To expand surgical options for safe, minimally invasive microsurgical procedures or targeted delivery of diverse therapeutics, a novel untethered micro-robotic platform is presented. This technology enables precision travel to predetermined central nervous system (CNS) parenchymal and complex cerebrospinal fluid pathway targets.

Methods: Utilizing an *in vivo* ovine model, gross pathological and microscopic histopathological brain tissue reactions to the navigation of this micro-robot were compared to inserting standard neurosurgical catheters, routed from an occipital burr hole to the frontal lobe and then returning. Descriptions of the evolving tissue responses were documented at 24 h, 2, 12, and 26 weeks following the procedures.

Results: No deaths or surgical complications occurred in either group. No neurological or behavioral differences were identified between the groups. No significant differences in gross or microscopic tissue pathology were identified when comparing the channels created by the micro-robot to the catheter control group.

Conclusion: These findings support the equivalence of tissue responses to this micro-robot navigation compared to catheter insertion as a preliminary surrogate for addressing the safety and accuracy of this novel platform. This platform may set a new standard for safe, anatomically precise, and minimally invasive therapeutic procedures. The described approach offers untethered navigation, capable of traversing CNS tissues in controlled, complex, curvilinear trajectories. Preliminary results utilizing this micro-robotic capacity to deliver diverse therapeutic payloads are discussed. Novel applications designed to address CNS pathologies, including neurodegenerative diseases, epilepsy, neuro-oncology, and functional and microsurgical procedures, are proposed.

Keywords: Bionaut, Blood-brain barrier, Cerebrospinal fluid navigation, Intraparenchymal navigation, Micro-robot, Parenchymal channeling

This is an open-access article distributed under the terms of the Creative Commons Attribution-Non Commercial-Share Alike 4.0 License, which allows others to remix, transform, and build upon the work non-commercially, as long as the author is credited and the new creations are licensed under the identical terms.

©2025 Published by Scientific Scholar on behalf of Surgical Neurology International

INTRODUCTION

General surgical approaches to the brain have remained largely unchanged over many decades. Classic entry portals defined by pioneers such as Cushing, Horsley, and Dandy a century ago^[2,10] remain challenging, and safe brain access still requires lengthy, multi-stage, and complex techniques. A related outstanding obstacle for advancing neurosciences remains the challenges associated with limited access to entry of novel local diagnostic monitoring strategies and delivery of diverse therapeutic modalities into the brain. Systemic delivery of therapeutics into the central nervous system (CNS) is frequently limited by the blood-brain barrier (BBB).^[6,19,20] Whereas optimization of the dose and regimen to increase therapeutic plasma concentrations may improve brain tissue levels, the effect is frequently hampered by the limited bioavailability, immune response, and, most significantly, by the off-target effects, which often translate into dose limiting toxicities. Multiple optimization techniques have been pursued to achieve molecular modifications of small molecules, biologics, and viral and cell-based therapies to enhance their transit across the BBB.^[25] Representative biochemical approaches are exemplified by fine-tuning lipophilic, hydrogen bonding, specific BBB receptor affinity properties of therapeutic modalities, as well as designing targeted delivery vesicles, including liposomes, endosomes, lipid, or polymer nanoparticles.^[12,17] Viral vector capsid modifications have been described which yield improvements in crossing BBB for increased transgene delivery efficiency.^[15,24] Specific biophysical protocols dating back decades designed to improve brain delivery have focused on transient disruption of the BBB. Strategies, such as osmotic shock and high intensity focused ultrasound (HIFU)/microbubble, have been described with encouraging animal studies yet have offered limited positive proof of concept in clinical applications.^[1,8,19,28] However, it must be remembered that crossing the BBB is only the first step toward achieving therapeutic doses for deep brain targets.

Approaches based on direct access of CNS *through* the intrathecal space, including ventricular, cisterna magna, and lumbar cistern, have revived attention to the delivery of diverse therapeutics, including targeted biologics.^[15,16] While attractive at first consideration, intrathecal drug delivery poses its unique challenges. Therapeutics delivered into the intrathecal space are subject to immediate dilution within the cerebrospinal fluid (CSF) as well as being subject to variable patterns of distribution and clearance, resulting in frequent (sub)systemic distribution and even off target liver and kidney effects. Ongoing studies into understanding the complex patterns of dispersion of therapeutics introduced into the intrathecal spaces may prove insightful, allowing for improved optimization of targeting. Redistribution patterns for therapeutics delivered intrathecally into the CNS are still

affected by a multitude of physiological barriers, including arachnoid cisterns, pial and/or ependymal surfaces, and risk of being counter-balanced by the CSF flow. Although lacking the barrier arising from the tight-junction architecture encountered at the BBB interface, these boundaries also represent physical barriers to passive diffusion. Characteristics affecting translocation from CNS across these boundary membranes and parenchymal distribution include the molecular size, lipophilicity, conformation, and charge characteristics of the moiety, frequently favoring smaller modalities versus larger moieties such as antibodies or virions.

Local delivery of therapeutics “where it’s needed” directly into the brain parenchyma is a relatively novel, rapidly developing area of both experimental and clinical research. Convection-enhanced delivery (CED) of both small molecules and biological agents has gained significant approval, representing a well-tolerated and efficacious delivery system for very specific clinical applications. However, several limitations associated with this technique include the relatively invasive nature of the treatment, constrained linear (straight line of sight) access to the treatment locus dictated by the selected entry point, and the geometry of the catheter, impacting the intervening healthy tissue traversed in route. Challenges unique to stereotactic needle placement and CED infusions include difficulty controlling backflow along the insertion tract and interstitial “escape” routes for therapeutics that limit dose tissue exposure and may still result in sub systemic adverse effects. Efforts to improve catheter design and perfusion parameters for clinical CED applications remain major areas of design and protocol development focus to achieve optimization.^[14,15,26]

To tackle these challenges, we are developing a novel approach for safe and reliable treatment of the targeted brain tissue. Specifically, we assembled a platform that comprises discrete, untethered, magnetically actuated particle(s), “Bionauts.” Bionauts are navigated in a complex yet predictable manner through CSF and/or brain tissues controlled by an external magnetic propulsion system (MPS). Bionauts are capable of following complex curvilinear trajectories to reach predefined targets accurately. Whereas numerous similar attempts have been described,^[30] most report on *in vitro*, *ex vivo*, or small animal-based studies that involve movement in the endogenous anatomical lumens exemplified by vasculature or gut.^[4,13,29] For example, a magnetically propelled theragnostic particle, such as the “Gastric Pill,” was reported for the intragastric environment.^[27] Notably, during our initial evaluation of the Bionaut safety *in vivo* in the ovine brain, we noticed that the micro-robots mediate the formation of safe and predictable tracks (the “channels”). Intrigued by this observation, we conducted a series of studies to gain a better understanding of this phenomenon.

A preclinical and clinical literature review further suggests that diverse neurosurgical and therapeutic delivery techniques also create channel-like tracks in the brain parenchyma. These commonly used clinical practices are well-validated and display clearly established therapeutic benefits. Across all of these evaluated procedures, insertion depths range between a few mm and up to 15 cm, depending on the therapeutic target location.^[21] The primary trauma caused to the tissue on insertion of a solid object is reported to be microscopic tissue tearing and micro-hemorrhages, followed by the secondary tissue response to the primary trauma.^[23] The remodeling of the surrounding tissue on insertion of a mm-scale tool is an important consideration for safety because it can determine the long-term effect that may prove challenging to observe during relatively short study periods. Literature reporting on magnetic resonance imaging (MRI) and tissue biopsy data from multiple neurosurgical techniques reveal the formation of channels along the insertion trajectory.^[18] For example, several approved drug-delivery (CED) and diagnostic (biopsy) techniques require that a tool be inserted through the intervening brain tissue to reach the target. Other clinically validated devices (e.g., ventricular shunting, deep brain stimulation [DBS], and micro-dialysis) involve long-term implantation to achieve desired diagnostic or therapeutic effects. These procedures result in observable channels in traversed parenchyma. A review of the literature suggests that channels created by these clinical tools inserted in the brain do not result in significant neurological deficits. For reference, standard neurosurgical biopsy needles have outer diameters of 1.8–2.3 mm, whereas clinical CED and external ventricular drain (EVD) catheters can range from 1.65 mm to 3.3 mm or more.^[5,11]

Preclinical data on the microsurgery tool-mediated formation of channels and respective platforms are abundant. For example, <1 h long infusion through a 1.65 mm wide CED cannula was reported to leave a channel-like trace in the brain parenchyma of non-human primates.^[21] Similarly, short-term (<1 day implantation of a 1 mm wide) DBS electrode created a channel-like trace in cat brains.^[24] Furthermore, the brief insertion of a 1 mm wide delivery needle left a cavity in the mouse brain, which was discernable by the naked eye and visible in the microscopy images.^[23] Similarly, a narrower, 0.5 mm wide hollow needle yielded channels of measurable diameter in the rat brain.^[3]

In clinical practice, shunts, DBS electrodes, endoscopic third ventriculostomy, brain micro dialysis, CED, EVDs, and electroencephalography devices inserted into the brain tissue also display comparable dimensions.

Considering the complexity and sensitivity of the brain to physical interventions, our immediate research focused on evaluating comparative tissue effects of a microsurgical

application of the millimeter scale Bionauts in the brain of large animals to those left by “standard of care” procedures as reviewed above.

To establish brain tissue responses to Bionaut navigation over clinically relevant distances, the ovine (sheep) model was selected based on the larger size of the brain and similarities of the craniocervical junction when compared to porcine, canine, feline, or even non-human primate models.^[22]

Due to the highly accurate and safe non-linear travel options available in the CSF and brain, the Bionaut micro-robotic platform offers altogether new clinical opportunities, allowing for untethered navigation through CSF and tissues. The motion of the Bionaut is preplanned using preoperative imaging studies. Real-time intraoperative bi-planar fluoroscopic imaging (with the option for cone-beam computed tomography [CT]) is co-registered with the planning MRI 3D data at the time of surgery. These preoperative studies enable three-dimensional path control with real-time confirmation of the precision of travel and subsequent function throughout the procedure. Considering the different options for accessing the CNS (cisterna magna, lumbar cistern, and burr hole) and the ability to plan curvilinear trajectories in the CSF or tissues, the Bionaut platform offers access to CNS targets not generally achievable by other procedures.

Experimental design, procedure, and follow-up

For preliminary characterization of tissue response to intraparenchymal navigation in the ovine brain, burr holes were created at anatomically defined occipital entry points. Then, either the Bionaut micro-robots or standard neurosurgical tools, such as EVD catheters or obturators, were navigated at approximate distances of 4 cm toward the frontal lobe, followed by extraction through return travel tracking through the same channel to the collection (insertion) point.

Survival time points following the procedures were selected for 1, 14, 90, and 180 days for both Bionaut micro-robot experimental devices and standard tools. Sample size groups of $n = 3$ were designated for each group. For the control 1-, 14-, and 90-day groups, a Medtronic ARES antibiotic impregnated 2.5 mm Ventricular Drainage Catheter (Ref: 911010) was selected. Of note, the chronic 180-day group was repeated after the completion of the shorter period groups, selecting the larger diameter obturator from a Braun 10 Fr (3.2 mm) peelable introducer (Ref: FH603SU), which was considered to be more relevant as a control device, with a similar outer diameter to that of the micro-robot. Using only the blunt rounded-tip obturator, it has an outer diameter of 3.1 mm, more closely matching the diameter of the threads of the Bionaut micro-robot.

Post procedure follow-up and examinations

Study animals were examined daily for neurological status/deficits and observable differences in their general behaviors (including activity levels, feeding, and socialization) for all groups (24 h–6 months).

On the scheduled sacrifice date, animals were euthanized by institutional review board (IRB) established protocol. Brains were immediately harvested and processed for gross and microscopic examination. Specimens were processed at MD Biosciences, Innovalora, Rehovot, Israel. Specimens were evaluated and reported on by an independent pathologist (Ori Brenner, BVSc Diplomate, American College of Veterinary Pathologists). For the primary review, the pathologist was blinded to the nature of the treatment groups that created the described channels. In addition to identifying any macroscopic pathology, gross examinations identified the tracks generated by either the catheter or micro-robot. Localizing the cavities in these gross tissue blocks guided subsequent handling to focus on microscopic visualization of the lumen and periluminal tissue changes. Specimens were sectioned, and hematoxylin and eosin were stained for microscopic evaluation of histopathology in the standard fashion.^[7] Data were collected as high-resolution micrographs, and measurements were recorded in tables. Following the completion of this documentation process, the pathologist reported unblinded summaries of the groups. The results present a means of assessing comparative tissue reactions to the two device types for long-distance travel through parenchyma.

MATERIALS AND METHODS

The Bionaut system

The Bionaut platform has been designed around an interconnected modular architecture consisting of the Bionaut micro-robots, an introducer and retrieval kit, and the MPS.

The Bionaut micro-robots

Bionauts are miniature components ranging from 5 to 25 mm in length, depending on their function. The Bionauts are manufactured with reproducible 3-D printing, constructed with a cylindrical cavity to accommodate a permanent Neodymium N52 magnet, and surrounded by a biocompatible shell, as shown in Figure 1 below.

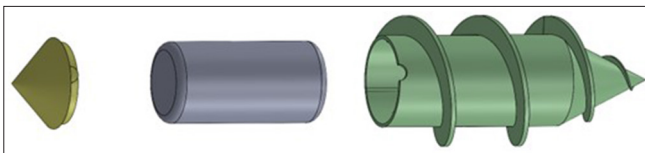


Figure 1: Enlarged view of Bionaut body, magnet, and end cap.

A “corkscrew” helical micro-robot (3.1 mm outer diameter, 1.625 cm length) used in this study benefits from the decreased demand for torque to allow motion through brain tissues propelled by an external magnetic array requiring a field strength of <0.1 Tesla. The nature of the polarity of the incorporated magnet can be varied, providing freedom for the implementation of diverse applications ranging from device only applications such as microsurgical or biopsy functionality to complex device-drug delivery options [Figures 1 and 2]. Variations in the design of the micro-robots allow for payload chambers for drug delivery, tissue biopsy, micro-electronics, and chemo-sensing functions.

The Bionaut introducer kit

The instruments kit contains four items: the Cannula, the Trocar, the Introducer (which includes a preloaded Bionaut), and the Retriever [Figure 3]. For this experiment, the full introducer kit (described below) was not used for these studies. Complete single-use sterile packs were used in all Good Lab Practices (GLP) and usability studies.

1. The cannula has an outer diameter of 4.0mm, an inner diameter of 3.8 mm, and a length of 12.3 cm from the distal edge of the handle. It accepts all three of the other components, which are 3.6–3.7 mm in outer diameter, and provides a locking mechanism using a “luer-lock” connector. The cannula has a coiled wire “stop” with an adjustable position, which is set to reduce the risk of penetrating too far at the skull base.
2. The Trocar has a three-bevel tip, oriented with the point “down” as it’s inserted into the cannula. In conjunction with the cannula, it allows for controlled penetration into the intrathecal space at the cisterna magna. Once the cannula is in place, the trocar is removed, and the internal seals of the cannula prevent the free flow egress of CSF.
3. The introducer carries the pre-loaded Bionaut into and through the cannula with a two-stage magnetic holding mechanism. The “hard hold” uses a pair of magnets to keep the Bionaut firmly retained inside the introducer lumen during processing, shipping, and introduction.

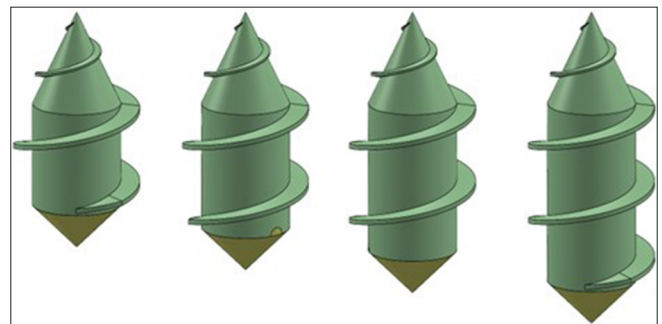


Figure 2: Various Bionaut length configurations of the “cork screw” version.

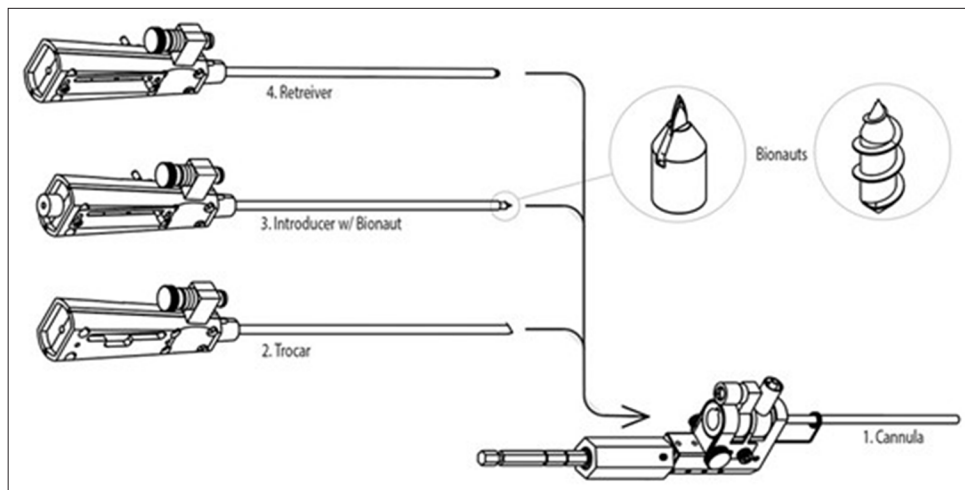


Figure 3: Schematic diagram of the Bionaut instruments set.

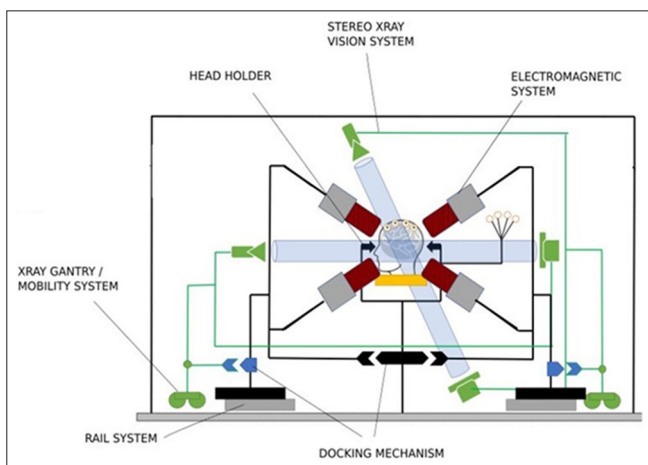


Figure 4: Schematic diagram of the Bionaut system. The Hardware controller graphical user interface (GUI) interface and power supply are not represented.



Figure 5: Illustrations of Medtronic's ARES antibiotic impregnated external ventricular drain catheter compared to Bionaut "screw bot" used for the 24 h, 2 week, and 3-month groups.

One magnet is fixed, and the other is removable. Once the introducer is in place inside the cannula, the "chaser" magnet can be withdrawn, greatly reducing the magnetic hold and allowing the MPS to take over control of the orientation and motion of the Bionaut.

4. The Retriever, post procedure, also passes through the cannula and has a magnetic tip. On completion of its task, the MPS guides the micro-robot back for capture by the retriever's magnetic tip. This allows for safe retrieval and extraction of the Bionaut through the cannula.

The MPS

The MPS system (version 2 used in this study as described in the schematic [Figure 4], with version 3 used for all subsequent GLP and useability studies) consists of eight fixed electromagnetic coils arrayed around the head. The electromagnetic system offers several advantages over permanent magnet systems, including greater flexibility of control for improved accuracy, faster response times, and the benefits of an on-off state for the system, which provides enhanced safety during the procedure and simplifies storage, setup, and disassembly of the unit. The MPS is controlled by a hardware and software system that executes pre-planned navigation created on the Bionaut planning software. The software uploads patient imaging data (CT, MRI) for planning purposes and then controls the magnetic field generated by MPS with feedback information from the biplane fluoroscopy Tracking System.

The tracking system is a subsystem of the MPS

The tracking system uses video output from a standard clinical biplanar diagnostic/interventional fluoroscopy installation. It provides closed-loop motion control feedback by providing the MPS controller with real-time 3D detection of the micro-robot location. This is calculated through simultaneous 2D positioning in orthogonal views, allowing for triangulation to determine the exact 3D location. The Bionaut's position is then overlaid in a 3D model of the brain sourced by pre-procedure MRI, allowing for continuous verification of the precision of navigation.

The graphical user interface is another subsystem of the MPS

This system is designed for interfacing end-user communication with the functionality of the Bionaut micro-robot and the MPS system. Based on preoperative

3D imaging and procedural planning, all phases of this plan are tracked in real-time with visualization of the progress of Bionaut navigation utilizing existing commercial biplanar/orthogonal fluoroscopic systems.

Animal models

Large animal model

Ovine studies were conducted at Sheba Research Hospital, Israel. Assaf breeds Sheep, 35–45 kg, were entered into either the Bionaut experimental group or the standard brain catheter control groups with $n = 3$ animals per group. All animals experienced induction of general anesthesia and intubation, followed by either the control catheter or the experimental Bionaut procedures, and then were allowed to recover for 24 h, 2 weeks, 3 months, or 6 months before scheduled sacrifice for pathological studies.

Animal model preparation

For this study, an occipital burr-hole was created and the dura opened to expose parenchyma in the standard manner. Post procedure, in all cases, the surgical site was closed in the usual fashion.

Time control points

Four survival time point groups were initiated for the first three shorter periods of 24 h, 2 weeks, and 3 months using a 2.5 mm EVD catheter as a control. Moreover, the longer 6-month survival used a larger 3.1 mm rounded blunt tip obturator.

Selection of appropriate experimental comparison

The Bionauts used were a minor body diameter of 2.8 mm and thread peak diameter of 3.1 mm outer diameter (O.D.). Neurosurgical catheters and introducers were selected to be roughly equivalent to the minor diameter. For the 24 h, 2 weeks, and 3 month cohorts, 2.5 mm outer diameter EVD catheters (Medtronic ARES, Ref 91101) were chosen [Figure 5]. For longer-term survival, a larger sheath's obturator (Braun 10 Fr Introducer (Ref: FH603SU)) of 3.1 mm outer diameter was selected.

Experimental devices and control devices

Experimental devices for insertion and retraction (Bionaut microbots)

For the experimental groups, either a “standard pitch” (2.0 mm thread pitch) (24 h, 14 days, 3 months, 6 months post-treatment evaluation cohorts) or “Long Pitch” (2.5 mm thread pitch [6 months post-treatment evaluation cohort]) Bionaut was used. The “corkscrew” Bionaut was manually

inserted into the occipital burr hole, navigated through the MPS under real-time fluoroscopy to the frontal lobe along the same trajectory used for the control groups catheters, and then navigated back to the burr hole for extraction. Specific details are summarized in Figure 6.

Control devices for insertion and retraction

For the control group in the shorter periods, either a Medtronic ARES EVD catheter (Ref #91101) [Figure 7] was inserted (2.5 mm outer diameter) for the 24 h, 2-week, and 3-month survival groups] or in the 6-month group the bare obturator from a Braun 10Fr insertion sheath peel-away cannula system (Ref: FH603SU) [Figure 8] (3.1 mm outer diameter for the 6-month survival group) were deployed. For both shorter-term and longer-term cases, the control catheter was carefully inserted under fluoroscopy to a depth of 4–5 cm toward the frontal lobe and then withdrawn.

RESULTS

Summary results

Neurologic Status: No neurological deficits were identified in either the catheter or the Bionaut groups throughout the study, extending from immediate postoperative evaluation to the 6-month follow-up. This included documentation of activity levels, feeding, socialization, etc. No fixed neurological deficits were appreciated in either group. No deaths occurred in either group.

Gross pathology

Thick section gross anatomy was reviewed postoperatively at 24 h, 2 weeks, 3 months, and 6 months points. Attention was focused on identifying the residual lumen and peri-luminal regional changes resulting from the passage of either the catheter or the Bionaut. No gross hemorrhage was observed in either group. No evidence of cerebral infarction/stroke was identified in either group. Over the time course, the residual lumen caused by either the catheter or Bionaut travel was found to decrease in size progressively. During the 6-month time course, the tract caused by either the Bionaut or catheter was difficult to identify in some sections.

Microscopic evaluation of tissues following catheter or micro-robot navigation in brain parenchyma

Postoperative tissue damage following either catheter

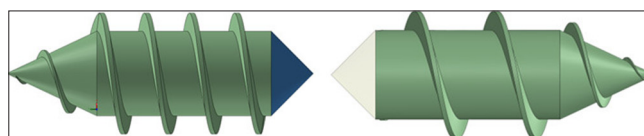
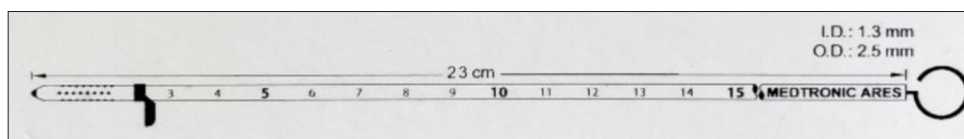


Figure 6: Standard pitch and long pitch Bionaut screw bots.

Table 1: Summary table for 14-day animals.

	Obturator			Bionaut		
Swine Tag	183	189	196	184	1553	1561
Gross ¹	-	-	-	+	+	+
Hole size ²	Small	Small	Medium	Large	Medium	Large
Location	WM-2/5	WM-1/3	WM-1/8	WM-2/6	WM-5/6	WM-2/8
	GM-2/5	GM-2/3	GM-1/8	GM-1/6	GM-1+/6	GM-5/8
	GWMJ-1/5		GWMJ-6/8	GWMJ-3/6		GWMJ-1/8
Surrounding tissue	Typical ³ , to max 0.5 mm	Typical, to max 0.5 mm	Typical, to max 0.3 mm	Typical, to max 1.2 mm	Typical, to max 0.5 mm	Typical, to max 0.5 mm

WM: White matter, GM: Gray matter, GWMJ: Gray white matter junction. ¹Gross lesions were evaluated in photos only and did not include the entrance/exit points identified at tissue trimming. ²This estimate considers the size of the largest holes. More precise evaluation can be done with morphometry. ³Typical changes include gliosis, pallor, vacuolation, vascular hypertrophy and hyperplasia, infiltration of macrophages (Gitter cells), fibrovascular proliferation, etc.

**Figure 7:** Control catheter for shorter term implants; Medtronic ARES antibiotic impregnated 2.5 mm ventricular drainage catheter.

tracts or micro-robot tracts was found to be consistent with previous descriptions based on the time course following the procedure. Acute inflammatory changes with microhemorrhages were appreciated in the 24 h and 2 week groups. At 3 months, inflammatory changes were much less prevalent. Gliosis was identified, bordering the lumen in both groups. This trend was more pronounced at the 6-month chronic time point with little inflammatory response remaining and gliosis documented in all sections. Pathology review found that both groups exhibited equivalent reactions and responses to the inciting insult.

Rather than include all the experimental data, the example of 14-day data is in Table 1.

24 h study results

Summary catheter control at 24 h

In our evaluation of the microtrauma created by both the surgical catheter and the Bionaut, the lesion shown in Figure 9 is representative of the 24-hour control tissue changes. It consists of a small central tear immediately surrounded by necro-hemorrhagic tissue and a wider region of vacuolated tissue, which measures approximately 2.1×1.3 mm in diameter.

Twenty-four hour post-Bionaut treatment summary

Gross findings correlate well with microscopic lesions. The microscopic lesions were similar in all samples [Figure 10].

They are characterized by an area of tissue loss exhibiting an irregular shape consistent with the cavity. This is surrounded by tissue showing variable necrosis, hemorrhage, vacuolation, and scattered spheroids. The lesions range from 34×2.1 mm to 7.6×4.7 mm. They are characterized by an area of tissue loss of irregular shape, which is surrounded by tissue showing variable necrosis, hemorrhage, vacuolation, and scattered spheroids. The largest lesion is 7.6×4.7 mm [Figure 9], and the smallest is 3.4×2.1 mm. The tissues are viable.

14 day study results

Summary catheter treatment control at 14 days

The residual lumens resulting from the passage of a catheter exhibit elongated, triangular, or cup shapes and range from 0.63×0.48 to 1.7×0.45 mm. Representative sections are presented [Figures 11 and 12]. The lumens contain variable numbers of infiltrating macrophages. The changes surrounding the cavity are similar and consist of vascular hypertrophy and hyperplasia, moderate vacuolation, and gliosis of variable degrees. Notably, they are more prominent in the gray matter sections than in the white matter. The tissue reaction surrounding the cavity extends to a maximum of 500 μ m from the hole.

Summary of post-Bionaut treatment at 14-days

Typical sections are presented in Figures 13 and 14. The cavity varies in shape from oval or tear-shaped to irregular



Figure 8: Control device for 6 month sheep; Braun 10 Fr (3.2 mm) inner diameter peelable introducer cannula, using only the blunt rounded-tip obturator with an outer diameter of 3.1mm, not including the sheath (Ref: FH603SU).

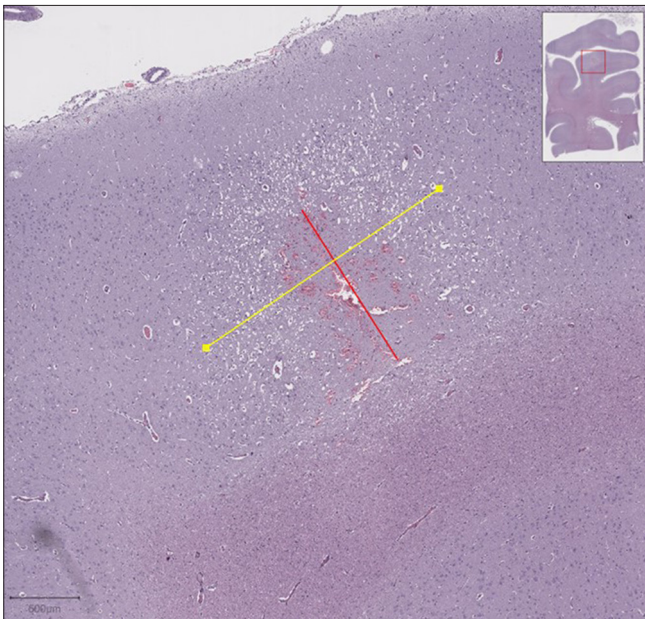


Figure 9: 24-h post-catheter treatment: The upper right window displays the gross pathology identifying the lumen. This typical cavity (red line) with surrounding tissue reaction (yellow line) consists of a thin margin of necro-hemorrhagic tissues and wider vacuolated tissues.

and ranges from 1.4×0.46 to 2.5×1.1 mm. It contains infiltrating macrophages and a very loose network of blood vessels. The reactive tissues surrounding the lumens ranging from 0.25 to 0.5 mm exhibit small changes, including varying degrees of loose networks of blood vessels, mild gliosis, and minimal vacuolation.

3 Month study results

Summary of 3-month post-catheter treated control

The lesions are similar to the findings at earlier time points [Figures 15 and 16] with signs of healing as evidenced by (i) smaller dimensions of the punctures, (ii) reduced number of pro-inflammatory cells, and (iii) rare and limited hemorrhage or microvasculature. They consist of a characteristic small cavity, most commonly narrow and

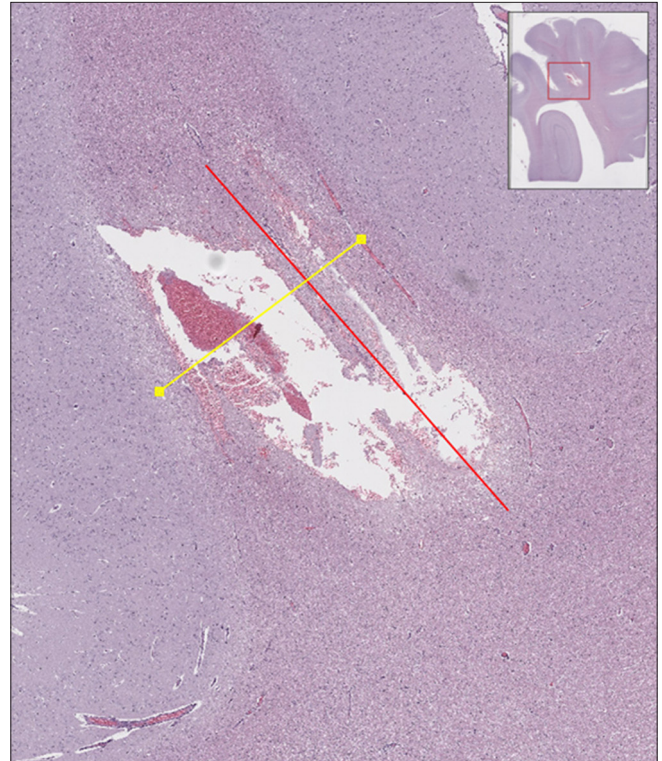


Figure 10: Twenty-Four h Bionaut: A typical slide exhibiting variable hemorrhage, necrosis, and vacuolation (yellow line) surrounding the lumen (red line).

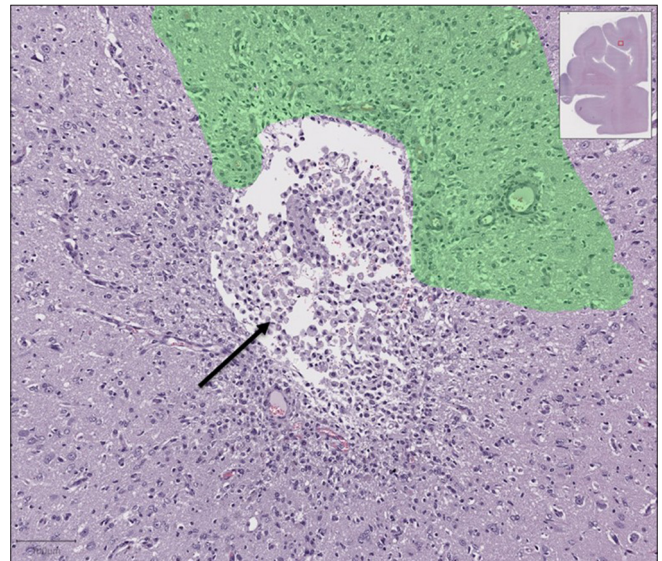


Figure 11: Fourteen-day catheter control: There is vascular hypertrophy and hyperplasia, (black arrow) vacuolation, and gliosis in the tissue surrounding the cavity. These changes involve an approximately 200–250 μm -wide band (partly shaded green to indicate its extent). The cavity is infiltrated with macrophages.

elongated, ranging between 0.9×0.5 and 1.6×0.3 mm. The lumens appear either optically empty or contain a few blood



Figure 12: Fourteen-day post-catheter treatment control: An approximately triangular hole (edges marked by black dots, $1,950 \times 570 \mu$) in the WM just below the gray-white matter junction (marked by a white dashed line). Surrounding tissue exhibits mild gliosis and vacuolation to $\pm 100 \mu$ m. The lumen displays an accumulation of macrophages (shaded yellow).

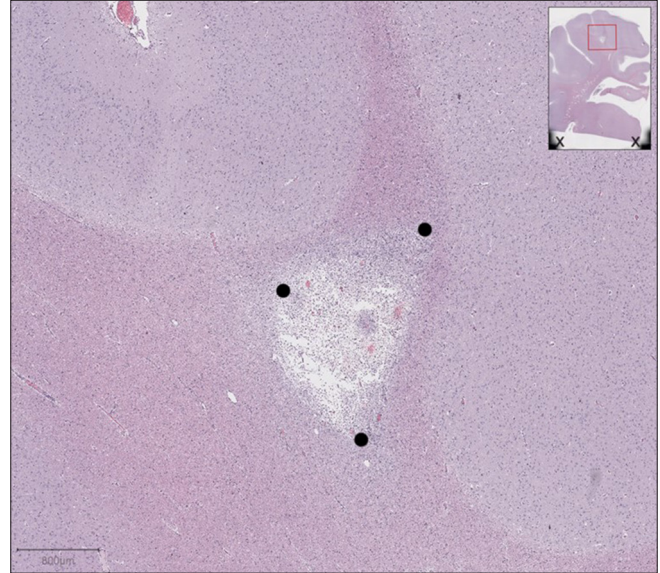


Figure 14: Fourteen day post-Bionaut treatment: A triangular shaped cavity bordered by black dots measures 2.1×1.3 mm. The cavity exhibits infiltrating macrophages. Surrounding tissue changes extend to 100μ m into the tissue surrounding the cavity and display mild gliosis and minimal vessel networks.

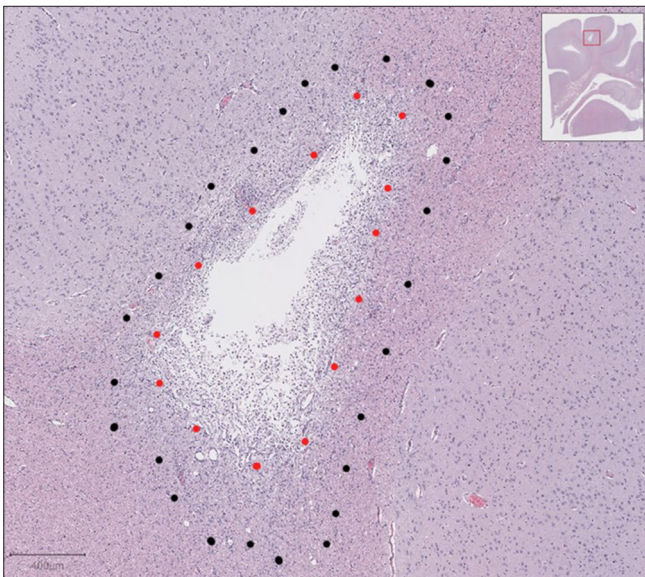


Figure 13: Fourteen day post-Bionaut treatment: Red dots mark the edges of the cavity measuring 1.97×0.81 mm, which contains infiltrating macrophages and loose blood vessels. Black dots encompass the tissue changes surrounding the cavity, with typical changes extending to approximately 250μ m.

vessels and/or mononuclear cells. The cavity is surrounded by a rim of gliosis, which is ± 0.3 mm wide.

Summary of ninety day post-Bionaut treatment

Lesions of similar morphology were identified in all samples [Figures 17 and 18]. Cavities contain loose fibrovascular tissue. The single lumens are somewhat larger than in the obturator control group, ranging from 1.5×1.3 to 2.7×1.0 mm, consistent with the larger outer diameter of the Bionaut (3.2 mm) compared to the Catheter control (2.5 mm). The cavities contain loose fibrovascular-like appearing tissue. Surrounding tissues exhibit mild gliosis, which interestingly appears to be less well-demarcated than in the catheter control group.

180 Day (6 months) study results

Six-month (180 days) post-standard Bionaut treatment

The residual cavities range from crescent-shaped to elongated and linear in shape and are surrounded by poorly demarcated tissue pale in appearance. The cavities range in size from 0.96×0.8 mm to 2.1×0.38 mm [Figures 19-21]. These cavities are largely optically empty or exhibit varying numbers of macrophages and very loose fibrillar tissue-collagen fibers [Figure 20]. Surrounding pale areas range from 0.5 to 0.7 mm and exhibit varying degrees of fibrillar-appearing glial processes, reactive astrocytes, gliosis, rare macrophages, lymphocytes, and blood vessels. The tissue displays clear signs of healing compared to microtrauma observed at 14 d and especially 24 h post-treatment. These

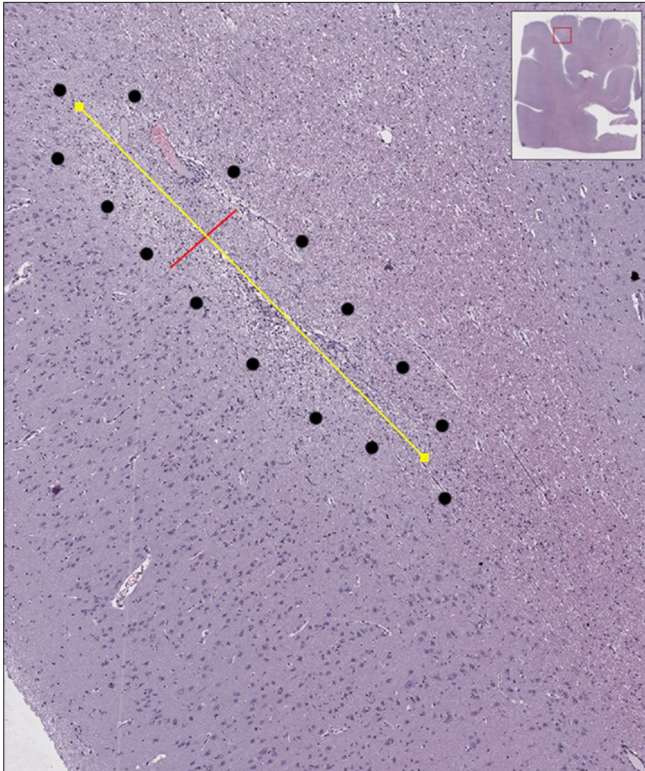


Figure 15: Ninety day post obturator treatment – A lesion (surrounded by black dots) in the gray matter near the gray matter and white matter junction. It consists of a small and elongated cavity (yellow marker measured 2.5 mm and red 0.7 mm, respectively), containing rare blood vessels, surrounded by a zone of gliosis about 0.3 mm wide. These lesions are the most common in this group and hence considered typical.

include the absence of residual hemorrhage, decline or, in some cases, complete absence of inflammatory cells, and evidence of gliosis.

180 days post-treatment with Bionaut

Six Month (180 days) Long Thread Pitch Bionaut treatment: Lesions exhibit findings typical to other groups [Figures 22 and 23]. Residual cavities ranged from 0.4×0.16 to 1.4×0.4 mm. Pale surrounding regions ranged from 0.4 to 0.8 mm in thickness and similarly exhibited gliosis and scant areas of mononuclear cell infiltration.

Six months (180 days) post obturator treatment control

The control group was generated using a 3.1 mm outer diameter obturator. Typical sections are presented [Figures 24 and 25]. Residual cavities ranged from 0.7×0.2 mm to 1.4×0.4 mm. Macrophage infiltrates can be identified in the cavities. The surrounding pale areas ranged from 0.4 to 0.8mm in thickness. Perivascular lymphocytic infiltration is rare.

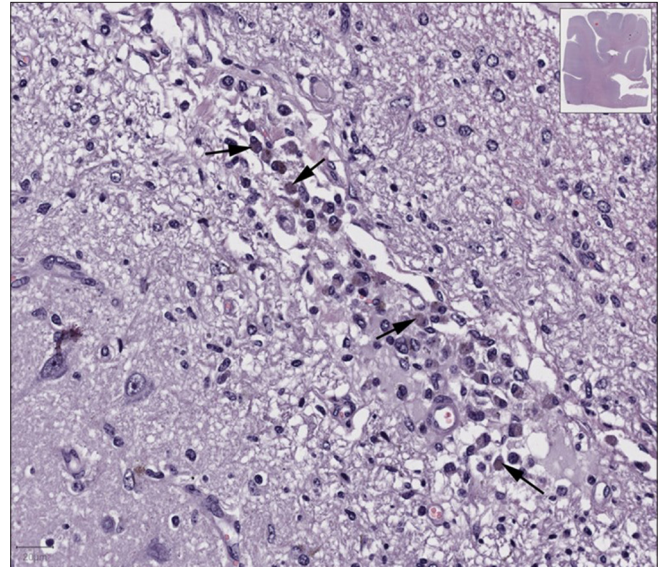


Figure 16: Ninety day post-obturator treatment. High magnification of the cellular infiltrates in the small cavity in the center of the previous lesion. Some of the infiltrating mononuclear cells (histiocytes) (black arrow) contain a small amount of brown granular pigment, presumably hemosiderin, potentially indicative of an unresolved microhemorrhage.

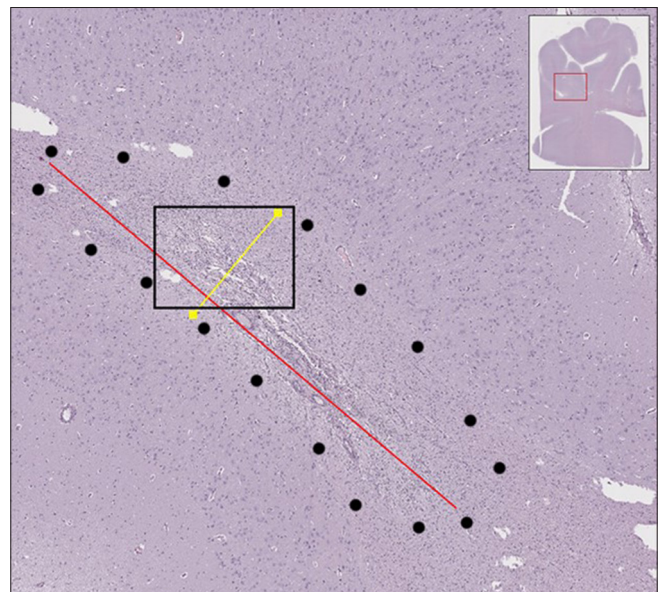


Figure 17: Ninety day post Bionaut treatment: Focal lesion delineated with red and yellow markers ($3.3 \text{ mm} \times 0.8 \text{ mm}$, respectively) in the white matter close to the gray-white matter junction. The lesion (outer edges marked with black dots) consists of an elongated and narrow cavity with irregular edges surrounded by diffuse gliosis.

DISCUSSION

The primary goal of this study was to evaluate and compare the biological tissue responses of Bionaut micro-robot

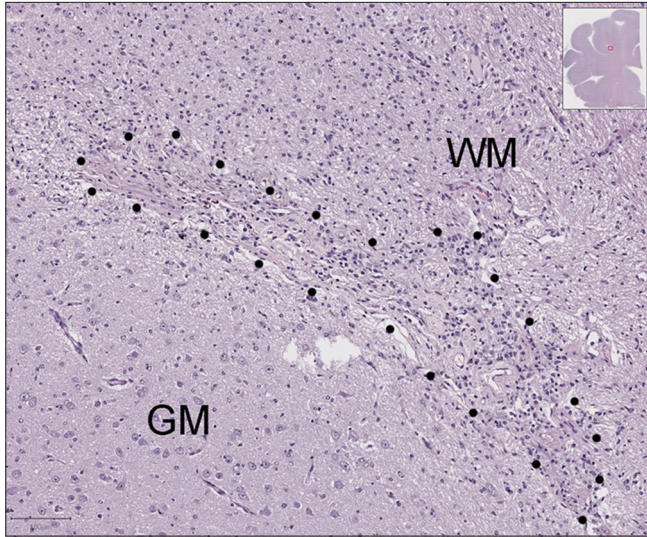


Figure 18: Ninety day post Bionaut treatment: The cavity is filled with loose fibrillar material, blood vessels, and mononuclear cells. Black dots mark the microtrauma boundaries with mild gliosis bordering the residual cavity, which is prominent in the white matter (WM) and mild in the gray matter (GM).

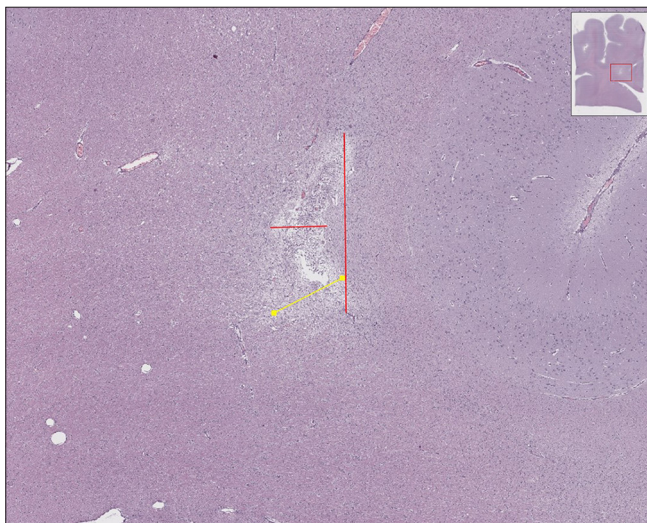


Figure 19: A representative sample at 180 days post Bionaut treatment: The cavity is crescent-shaped and surrounded by pale tissue. Dimensions (of pale tissue): 16.87×0.49 mm (red bars). The pale area is a little wider ventrally (0.71 mm, yellow bar).

movement through brain parenchyma as compared to the tissue response appreciated with typical neurosurgical device insertions. Neurological outcomes and tissue histopathological changes were compared to those seen with the passage of clinical brain catheters, such as the Medtronic ARES EVD catheter or the Braun 10 Fr Peelable sheath obturator, traversed along the same trajectories [Figure 8]. These results were related to the existing literature describing the nature and consequences of surgical procedures, which

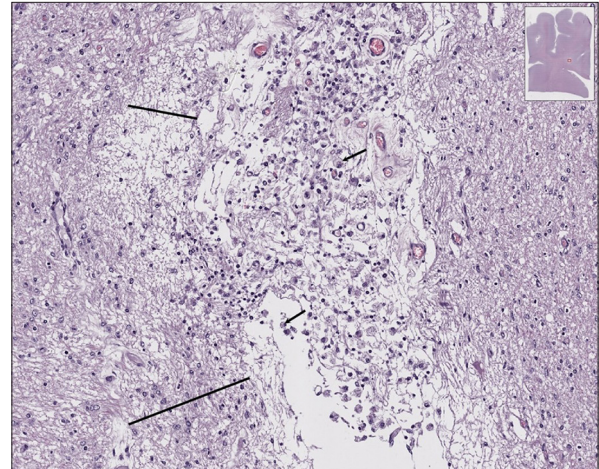


Figure 20: A representative 180 days post Bionaut treatment: The higher power magnification contents of the cavity are typical. Arrows: Macrophages. Black bars span pale tissue which is more vacuolated on top and more fibrillar at the bottom.

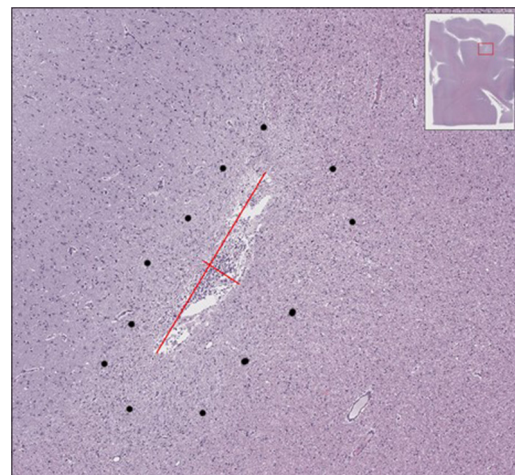


Figure 21: A representative 180 days post Bionaut treatment. A typical 1.07×0.21 mm cavity (red lines) surrounded by a thin pale band with outer edges marked with black dots exhibiting areas of mild gliosis and sparse mononuclear cells.

ultimately create channels through brain parenchyma and provoke sequential periluminal tissue responses.

The histopathological outcome of traversing surgical instrumentation of the mammalian brain is well documented. Acutely, piercing the brain parenchyma damages capillaries along the insertion trajectory, leading to leakage of blood components into the immediately adjacent parenchyma. This trauma results in micro-hemorrhage and localized inflammation, altered nutrient and oxygen supply, oxidative stress, and accumulation of toxic compounds. Within hours, microglia and astrocytes are activated by inflammatory

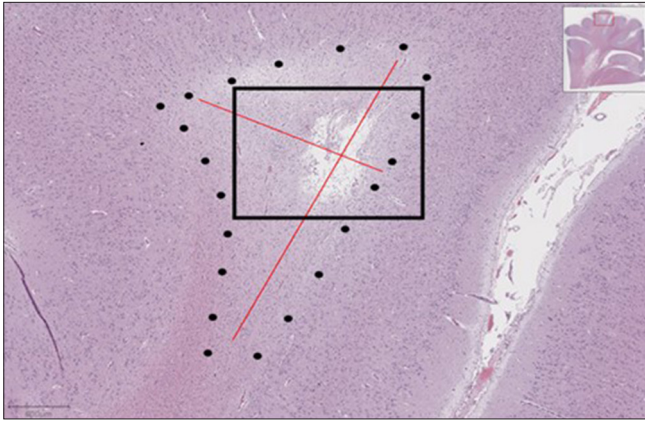


Figure 22: Six-month (180 days) post-long Bionaut treatment: A typical lesion in a dorsal gyrus is shown. The black dots encircle the pale gliotic area surrounding the cavity, measuring 3.2×1.7 mm in diameter (red lines). The boxed area is shown in the following higher magnification photo.

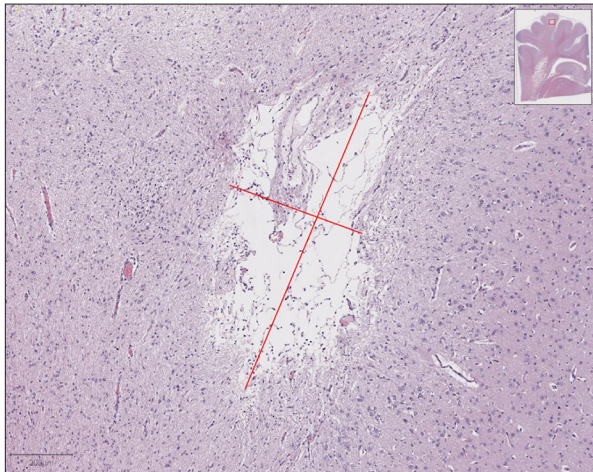


Figure 23: Six-month (180 days) post-long Bionaut treatment: The cavity is largely optically empty. It measures 1.04×0.46 mm (red lines) and is surrounded by a perimeter of gliosis.

signals and migrate toward the site of injury. Some adjacent neuronal loss results from these processes, while the surviving neurons may become transiently activated. Within days, reactive gliosis begins to replace the local inflammation and neuronal loss in the affected tissues.^[9]

As noted in the summary results, no gross deficits were identified in animals treated with either the catheter or the Bionaut throughout the study, extending from 24 h and up to 180 days post-operational follow-up. This included normal activity, feeding, socialization, grooming, etc. No treatment-associated neurological deficits were detected in either group throughout the studies. Surgical complications such as infection, CSF leaks, or deaths were not observed in either group. This reporting must be tempered with the understanding that resulting human reactions may be more sensitive to the different modes of tissue trauma. However, the long history of

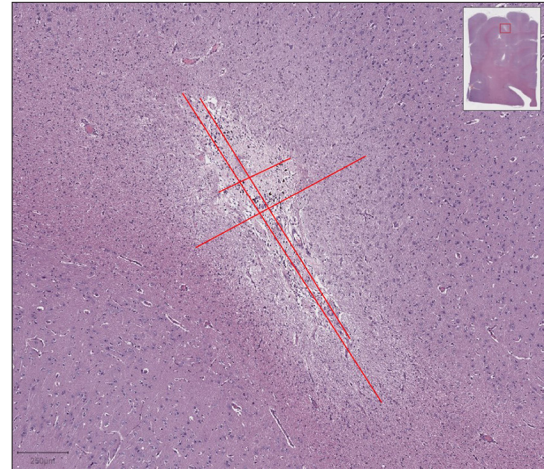


Figure 24: Six-month (180 days) post-obturator treatment control: Cavity of 1.4×0.4 mm in the white matter close to the gray-white matter junction is observed (2-long and 1-short perpendicular red line). The surrounding pale area measures 1.8×0.96 mm (long perpendicular red line). This residual pale area exhibits gliosis and limited mononuclear infiltration.

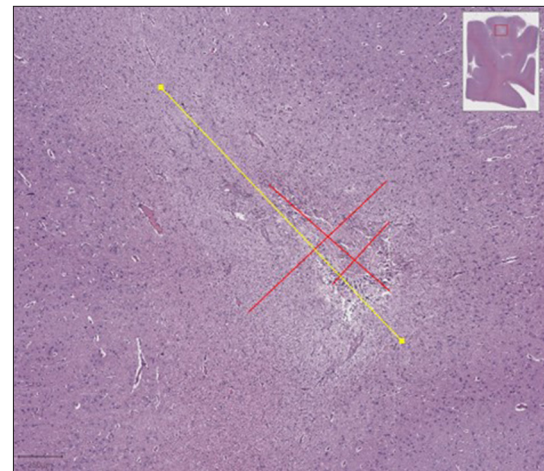


Figure 25: Six-month (180-day) post-obturator treatment: Cavity of 0.92×0.5 mm (red marker parallel to yellow and short perpendicular red marker) in white matter close to gray-white matter junction. Pale gliotic area: 2.0×1.01 mm (yellow and long perpendicular red marker).

safe temporary and chronic insertions of neurosurgical devices of diverse natures offers optimism, given the skilled utilization of the techniques and anatomy chosen for these devices.

There were no significant pathological findings in any group at any time point on review of the gross tissue examinations up to and including the 6-month groups. Cerebral infarction, hemorrhage, or inflammation were not detected in either group. Postoperative tissue damage following either the catheter tract or the Bionaut tract was found to be consistent

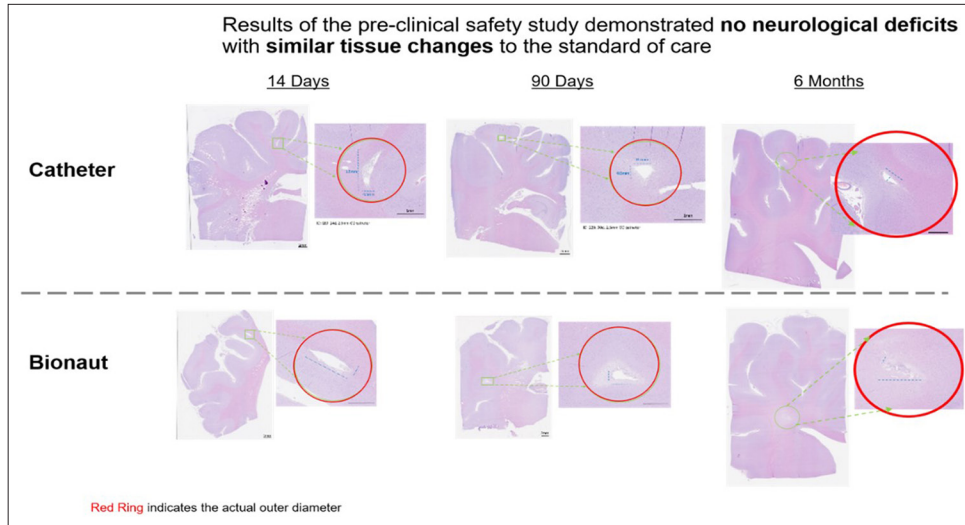


Figure 26: Tissue response to lesions induced by catheter or Bionaut are essentially equivalent over the various survival times. For perspective, the red circles represent the outer diameter dimensions of either the catheter or the Bionaut.

with previous descriptions based on the time course following the procedure. At 24 h post treatment, both devices produced small focal lesions, which consisted of a cavity surrounded by tissue showing variable hemorrhage, necrosis, and vacuolation. The surrounding changes proved to be limited in their extent. The composition and content of typical lesions differed only slightly between the two treatments. The Bionauts produced cavities of irregular shape, which contained variable amounts of hemorrhage and necrotic debris. Typical lesions comprised a central hole/tear, necrotic tissue, and changes in surrounding tissue (e.g., vacuolation induced by the catheter). These lesions were smaller than those induced by the respective Bionaut and consistent with the smaller diameter of the surgical catheter [2.5 mm] in comparison to the Bionaut [3.2 mm]). Interestingly, the catheter produced tissue changes that resembled tissue tears rather than the sharp-edged lumens resulting from the Bionaut treatment. In contrast, isolated areas of micro-hemorrhage were identified in the Bionaut-treated brain tissue. These tracks were consistent with the thread pattern of the corkscrew Bionaut and were considered to be of no pathological significance. The tissue reactions surrounding the propulsion tracks were otherwise equivalent between the two groups. This reporting by the pathologist may represent the differences between blunt tissue disruption by catheter tip penetration in contrast to the sharp cutting associated with the screw-bot sharp tip and threads.

Bionaut and control animals evaluated at 14 days following treatment exhibited similar findings, with the Bionaut generating slightly larger channels, which are consistent with the larger outer diameters of the micro-robots. In both groups, tissue reaction bordering the cavity did not extend beyond 0.5 mm.

At 3 months, channels resulting from the catheter control treatment remain slightly smaller than the Bionaut-made channels, a finding which remains consistent with their smaller outer diameters. The channels exhibited similar findings with variable mononuclear cell infiltrates and fibrovascular networks. Surrounding tissue reactions bordering the cavities exhibited gliosis and scarce mononuclear cell infiltration consistent with a waning inflammatory process. Acute inflammatory changes with microhemorrhages were noticeable at 24 h and 2-week groups only, whereas at 3 months, inflammatory changes were much less prevalent, and microhemorrhages had resolved. Interestingly, gliosis was often less well demarcated in the Bionaut group as compared to the control specimens at this time point.

At 180 days, regardless of the experimental micro-robot or the control procedure using the 3.1mm outer diameter obturator, typical lesions in the white matter consist of a channel of variable size and shape, which is surrounded by a band of pale, gliotic tissue. In some cases, the cavity is widely patent and is either optically empty or contains variable numbers of cells, usually macrophages. In other samples, the cavity can be identified, but it is largely or entirely covered by fibrillar tissue, which usually includes blood vessels and may or may not include mononuclear cells (lymphocytes and macrophages). In the gray matter, typical lesions are either a defect (i.e., tissue loss) or a scar surrounded by gliosis. The largest lesions are found in the dorsal gyri and involve both gray and white matter. These are presumably the insertion sites for the trocar or the insertion/entry and recovery/exit site for the Bionaut device. Lesions of similar appearance are seen in all groups. Thus, the size, shape, and location of the lesion in a given sample is determined by the specific experimental protocol but taken as a whole, the lesions are indistinguishable between groups. At this

late time point, inflammation is scant. Other than the presence of lesions, consistent findings were not identified (e.g., vascular or meningeal changes). At 180 days (6 months), evaluation, controls, and Bionaut lesions were indistinguishable.

After the blinded independent pathology evaluation, the nature of the treatment groups was subsequently revealed, essentially unblinding the mechanism to the independent pathology reviewer. Despite the differences in nature of the forces and the brain tissue propulsion modes that generated the cavities, namely, blunt tearing with catheter compared to the controlled coring associated with the Bionaut motion, closure of these healing dynamics of channels was concluded to follow similar time courses. For channels in gray matter, the 6-month chronic lesions appeared blander, exhibiting either tissue loss or a gliotic scar. At 6 months, peri-lesional inflammation was scant. White matter lesions appeared to exhibit more pronounced surrounding vascular proliferation and persistence of macrophage and lymphocytes. Notably, vascular changes or meningeal inflammation were not detected outside of the tissue immediately proximal to the created channels ca 200–500 μm [Figure 26].

CONCLUSION

These results correlate well with available *in vitro*, *ex vivo*, and *in vivo* data in rodents and non-human primates. Both independent and internal evaluation of the ovine data further suggest that neurological, gross pathological, and microscopic histopathological results of navigating a control catheter or the Bionaut are equivalent. Analysis of both clinical and late-stage preclinical data supports this proposed approach to navigate the Bionaut for microsurgical procedures or targeted drug delivery, benefiting from a similar favorable clinical safety profile compared to other methods of drug delivery into deep brain targets.

Published clinical and large animal studies data suggest several key observations: (i) it is generally accepted that clinical benefits can significantly outweigh the risks of inserting a millimeter scale object into select deep brain targets, (ii) all surgical tools and procedures leave a channel-like track in the parenchyma; (iii) tracks remain patent for various periods post-removal of the object, and (iv) there are no reports of adverse effects attributed to these residual channels when properly placed. In our view, similar non-linear channels created by the Bionaut are expected to display a comparable safety profile in the brain. We attribute this to several factors, including (i) careful control of forces and propulsion mode mediated by our MPS and software; (ii) the ability to carefully plan and execute a safe path to access the target respecting sensitive anatomy with curvilinear paths possible in three dimensions rather than being restricted to potentially suboptimal linear trajectories; (iii) control over topology, dimensions, and patency of the channel(s); and (iv) selection of a safe point of entry and recovery for the Bionaut. As previously discussed, the functionality of the

Bionaut platform offers diverse opportunities for accurately reaching otherwise difficult or inaccessible targets of the brain, spinal cord, and CSF pathways. This platform represents a new tool for understanding and intervening in the complexity of the brain and its pathologies, respectively. So far, the focus on successful local drug delivery has focused on macroscopic perspectives. *In vitro* testing is well underway for utilizing the payload carrying capacity of this system to deliver a clinically relevant dose of a therapeutic agent directly and exclusively to a predetermined CNS target. A leading goal for developing this system will be to achieve a “payload agnostic” delivery platform. We have already achieved positive metrics for the delivery of small molecules, molecular entities Ribonucleic Acids (RNAs) and anti-sense oligonucleotides (ASOs), and viral vectors (Adenovirus (ADV) and Adeno-associated virus (AADV) into rodent and large animal brains. Further development of the potential of this type of platform includes the opportunity for target tissue biopsy either independently or concomitantly at the time of delivery of the therapeutic agent.

The final challenge associated with targeted CNS drug delivery must address the complexities addressing the pharmacodynamics occurring in the microscopic realm of monitoring for CNS pathologies. Depending on the nature of the delivered therapeutic, understanding and managing aspects of the micro-environment must address the interstitial environment, cellular uptake mechanisms, extracellular and intracellular metabolism, and inflammatory and immune responses. The potential introduction of selectively targeted biochemical sensors offers novel opportunities to gain insight into the general process as well as patient specific feedback from responses to interventions. Just as our understanding has grown with the development of imaging technologies, from X-rays to angiograms, from CT to MRI, and MRI spectroscopy and functional studies, this platform may provide new opportunities for resolving many of these questions at the microscopic level.

Ethical approval: The research/study complied with the Helsinki Declaration of 1964.

Declaration of patient consent: Patient’s consent was not required as there are no patients in this study.

Financial support and sponsorship: Funding for this research came from the Mayo Clinic, the University of California Irvine, the Cleveland Clinic, and private funding.

Conflicts of interest: Michael Kardosh, Florent Cros, Olin J. Palmer, Alexander Kiselyov are the employees of Bionaut Labs Inc.

Use of artificial intelligence (AI)-assisted technology for manuscript preparation: The authors confirm that there was no use of artificial intelligence (AI)-assisted technology for assisting in the writing or editing of the manuscript and no images were manipulated using AI.

REFERENCES

1. Al-Ahmady ZS. Selective drug delivery approaches to lesioned brain through blood brain barrier disruption. *Expert Opin*

- Drug Deliv 2018;15:335-49.
2. Barker FG. The Massachusetts General Hospital: Early history and neurosurgery to 1939. *J Neurosurg* 1993;79:948-58.
 3. Bjugstad KB, Lampe K, Kern DS, Mahoney M. Biocompatibility of poly(ethylene glycol)-based hydrogels in the brain: An analysis of the glial response across space and time. *J Biomed Mater Res A*. 2010;95:79-91.
 4. Ceylan H, Yasa IC, Kilic U, Hu W, Sitti M. Translational prospects of untethered medical microrobots. *Prog Biomed Eng* 2019;1:012002.
 5. Clearpoint neuro, SmartFlow® cannula. Available from: <https://www.clearpointneuro.com/biologics-drug-delivery/smartflow-cannula> [Last accessed on 2024 Sep 05].
 6. de Boer AG, Gaillard PJ. Strategies to improve drug delivery across the blood-brain barrier. *Clin Pharmacokinet* 2007;46:553-76.
 7. Fischer AH, Jacobson KA, Rose J, Zeller R. Hematoxylin and eosin staining of tissue and cell sections. *CSH Protoc*. 2008 May 1;2008:pdb.prot4986. doi: 10.1101/pdb.prot4986.
 8. Gandhi K, Barzegar-Fallah A, Banstola A, Rizwan SB, Reynolds JN. Ultrasound-mediated blood-brain barrier disruption for drug delivery: A systematic review of protocols, efficacy, and safety outcomes from preclinical and clinical studies. *Pharmaceutics* 2022;14:833.
 9. Hamani C, Davidson B, Lipsman N, Abrahao A, Nestor SM, Rabin JS, *et al.* Insertional effect following electrode implantation: An underreported but important phenomenon. *Brain Commun* 2024;6:fcae093.
 10. Hansson N, Schlich T. Highly qualified loser? Harvey Cushing and the Nobel prize. *J Neurosurg* 2015;122:976-9.
 11. Integra lifesciences, cerebroflo EVD catheter. Available from: <https://products.integralife.com/ventricular-catheters/category/neurocritical-care-evd-catheters-ventricular-catheters> [Last accessed on 2024 Oct 02].
 12. Khaledian S, Dayani M, Fatahian A, Fatahian R, Martinez F. Efficiency of lipid-based nano drug delivery systems in crossing the blood-brain barrier: A review. *J Mol Liquids* 2022;346:118278.
 13. Koleoso M, Feng X, Xue Y, Li Q, Munshi T, Chen X. Micro/nanoscale magnetic robots for biomedical applications. *Mater Today Bio* 2020;8:100085.
 14. Lewis O, Woolley M, Johnson D, Rosser A, Barua NU, Bienemann AS, *et al.* Chronic, intermittent convection-enhanced delivery devices. *J Neurosci Methods* 2016;259:47-56.
 15. Liu D, Zhu M, Zhang Y, Diao Y. Crossing the blood-brain barrier with AAV vectors. *Metab Brain Dis* 2021;36:45-52.
 16. Lutters B, Koehler PJ. A road less travelled: The centenary of cisterna magna puncture. *Brain* 2020;143:2858-62.
 17. Masserini M. Nanoparticles for brain drug delivery. *Int Scholar Res Notices* 2013;2013:238428.
 18. Ogiwara T, Nitta J, Fujii Y, Watanabe G, Kuwabara H, Agata M, *et al.* A preliminary study of the diagnostic efficacy and safety of the novel boring biopsy for brain lesions. *Sci Rep* 2022;12:4387.
 19. Pandit R, Chen L, Götz J. The blood-brain barrier: Physiology and strategies for drug delivery. *Adv Drug Deliv Rev* 2020;165:1-14.
 20. Pardridge WM. A historical review of brain drug delivery. *Pharmaceutics* 2022;14:1283.
 21. Pocevičute R, Mitchell K, Nikolakopoulou AM, Cho SK, Ma X, Chen P, *et al.* Quantitative 3D reconstruction of viral vector distribution in rodent and ovine brain following local delivery. *Neuroimage Rep* 2024;4:100218.
 22. Royo J, Forkel SJ, Pouget P, Thiebaut de Schotten M. The squirrel monkey model in clinical neuroscience. *Neurosci Biobehav Rev* 2021;128:152-64.
 23. Salegio EA, Hancock K, Korszen S. Pre-clinical delivery of gene therapy products to the cerebrospinal fluid: Challenges and considerations for clinical translation. *Front Mol Neurosci* 2023;16:1248271.
 24. Song J, Li N, Xia Y, Gao Z, Zou SF, Kong L, *et al.* Arctigenin treatment protects against brain damage through an anti-inflammatory and anti-apoptotic mechanism after needle insertion. *Front Pharmacol* 2016;7:182.
 25. Terstappen GC, Meyer AH, Bell RD, Zhang W. Strategies for delivering therapeutics across the blood-brain barrier. *Nat Rev Drug Discov* 2021;20:362-83.
 26. Villalobos J, Fallon JB, McNeill PM, Allison RK, Bibari O, Williams CE, *et al.* Preclinical evaluation of a miniaturized Deep Brain Stimulation electrode lead. *Annu Int Conf IEEE Eng Med Biol Soc* 2015;2015:6908-11.
 27. Vogelbaum MA, Brewer C, Barnett GH, Mohammadi AM, Peereboom DM, Ahluwalia MS, *et al.* First-in-human evaluation of the Cleveland Multiport Catheter for convection-enhanced delivery of topotecan in recurrent high-grade glioma: Results of pilot trial 1. *J Neurosurg* 2018;130:476-85.
 28. Wang Q, Xu Y, Xue R, Fan J, Yu H, Guan J, *et al.* All-in-one theranostic platform based on hollow microcapsules for intragastric-targeting antiulcer drug delivery, CT imaging, and synergistically healing gastric ulcer. *Small* 2022;18:2104660.
 29. Wu D, Chen Q, Chen X, Han F, Chen Z, Wang Y. The blood-brain barrier: Structure, regulation, and drug delivery. *Signal Transduct Target Ther* 2023;8:217.
 30. Zheng L, Chen LG, Huang HB, Li XP, Zhang LL. An overview of magnetic micro-robot systems for biomedical applications. *Microsyst Technol* 2016;22:2371-87.

How to cite this article: Loudon W, Kardosh M, Cros F, Katznelson B, Shtein A, Fedotenko K, *et al.* Novel untethered micro-robotic platform developed for minimally invasive ultra-selective microsurgical procedures and targeted drug delivery: Preliminary characterization of tissue response to intraparenchymal navigation in ovine brain. *Surg Neurol Int*. 2025;16:157. doi: 10.25259/SNI_841_2024

Disclaimer

The views and opinions expressed in this article are those of the authors and do not necessarily reflect the official policy or position of the Journal or its management. The information contained in this article should not be considered to be medical advice; patients should consult their own physicians for advice as to their specific medical needs.